

# **The Design, Manufacture and Test of a Liquid Propellant Aerospike Rocket Engine**

**Submitted to the 2002 Engineering Student Design Competition  
June 14, 2002**

## 1.0 Introduction

### *1.1 The advantage of Spike Shaped Nozzles vs. conventional bell-shaped nozzles*

In a conventional bell-shaped nozzle, combustion gases flow through a constriction (throat) and then expand away from the centerline. The diverging walls of the nozzle up to the exit plane contain the expanded gases. Bells nozzles are a point design with optimum performance at one specific pressure, i.e. altitude. Careful design is needed to achieve desired high altitude performance while avoiding flow separation at the walls of the nozzle near the exit when operating at low altitudes, which can lead to loss of performance and possible structural failure of the nozzle due to dynamic loads.

Contrary to a bell-shaped nozzle, the gas flow of a spike nozzle is directed radially outward from an annulus at some diameter away from the centerline. This flow is directly exposed to ambient pressure and it expands to the external environment, providing continuous altitude compensation. This compensation allows for little loss of thrust at off-design altitudes, and safer dynamic loads at start-up.

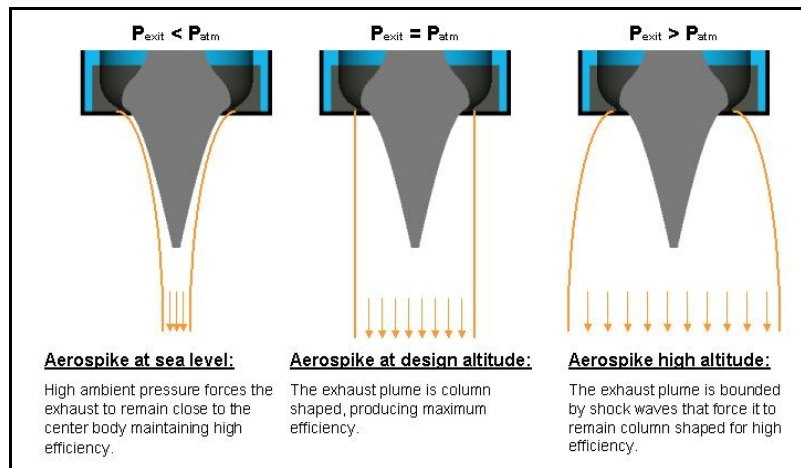


**Figure 1-Spike nozzle flow fields at various atmospheric pressures**

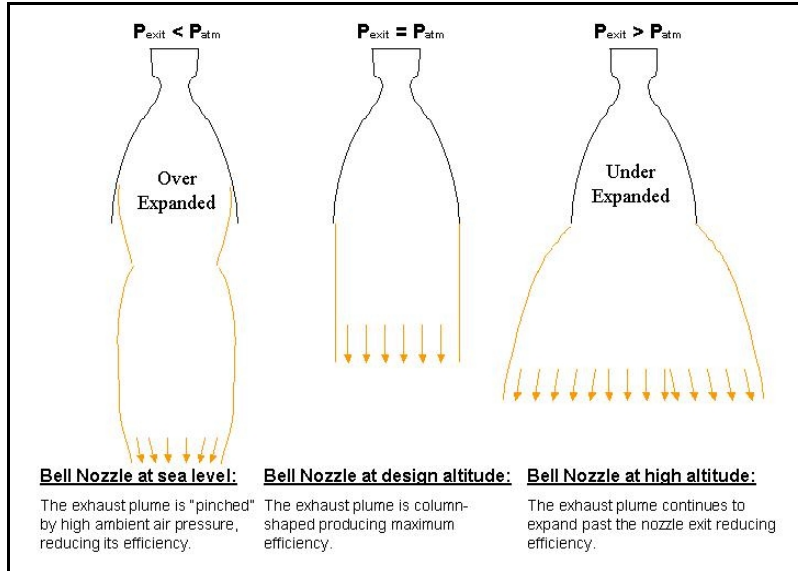


**Figure 2-Conventional nozzle flow fields at various atmospheric pressures**

### 1.2 Truncation

The ideal spike is truncated to save engine mass and required cooling area. This truncation results in a wake at the base of the spike, which induces some losses in performance. However, this can be offset by pumping secondary flow (about 1% of primary flow) into the base region to elongate the wake, thus forming an aerodynamic contour similar to the truncated structure (hence the name "aerospike").

### 1.3 History of the Aerospike

The aerospike concept is particularly advantageous for developing single stage to orbit (SSTO) vehicles due to its high efficiency at various altitudes. Aerospike engines were investigated by Rocketdyne in the 1960's, and then again as part of the now cancelled X-33 program. As part of the latter, Boeing Rocketdyne developed the RS-2200, a linear aerospike that was static fired several times. However, after more than four decades of research, no aerospike engine is known to have powered a rocket in flight.

### 1.4 How thrust is produced

An important equation, derived from the conservation of momentum, helps to understand what influences the thrust of a rocket engine (eq. 1):

$$F_{Thrust} = \dot{m}^* V_{ex} + A_{exit} (P_{exit} - P_{atm}) \quad (eq. 1)$$

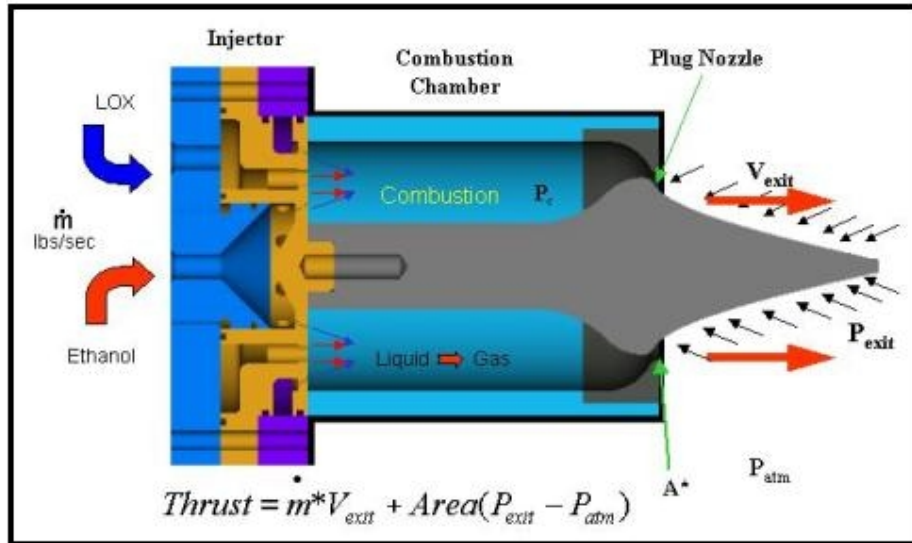


Figure 3

The term  $\dot{m}$  is the mass flow rate of the propellants, which is controlled by the orifice sizes in the injector. The velocity of the exhaust gases,  $V_{ex}$ , is a function of the area of the nozzle's throat and how the nozzle performs. The cross-sectional area of the nozzle at the exit,  $A_{exit}$ , is found by determining the area needed to expand the exhaust gases so that the exit pressure is equal to the atmospheric pressure at the design altitude. In general,  $P_{exit}$ , the pressure of the gases at the exit of the nozzle differs from  $P_{atm}$ , the ambient pressure around the rocket engine at its given altitude. The design of the rocket engine's injector, combustion chamber, and nozzle has an effect on all of these terms.

### 1.5 Objectives of the project

The goal of flying the first aerospike-powered rocket was taken on as the senior design project for the Aerospace System Design I & II course. Through the state-funded California Launch Vehicle Education Initiative (CALVEIN), and with help from aerospace professionals, students were set to develop a 1000 lb<sub>f</sub> annular, ablative aerospike rocket engine using liquid oxygen (LOX) as the oxidizer and ethanol as the fuel. Over the course of two semesters the initial requirements were flowed down throughout all of the components of the aerospike engine, shaping the final design. Once built and flight qualified through a static fire, the first powered flight of an Aerospike engine would take flight on the already developed Prospector-2 rocket (also built by students).

In the following sections the design process, manufacturing, and testing of the aerospike engine will be described and the results shown.

## 2.0 Design Process

### 2.1 Requirements

The process of designing the engine was the most arduous phase of development because the initial design requirements, which are the desired thrust of the engine, the

propellants that would be used, and the use of an aerospike for a nozzle, had to be considered. Because the engine would be integrated to the Prospector-2 rocket, the use of denatured ethanol and liquid oxygen (LOX) for propellants, and a maximum tank pressure of 390 psi were already determined. One of the initial requirements specified that the engine must burn for a duration of 6 seconds. This created the need for some type of cooling on the walls of the combustion chamber and the spike. The decision was made to use film cooling on these surfaces.

### *2.2 Design Drivers and Preliminary Design*

The main design driver was the configuration of the injector(s) with respect to the aerospike element. In the past, most aerospike engines incorporated an array of thrusters around the spike element, mainly to prevent combustion instabilities. In order to decrease manufacturing time and the complexity of plumbing, it was decided that the spike element would be attached to the face of one injector as shown in Figure 4.

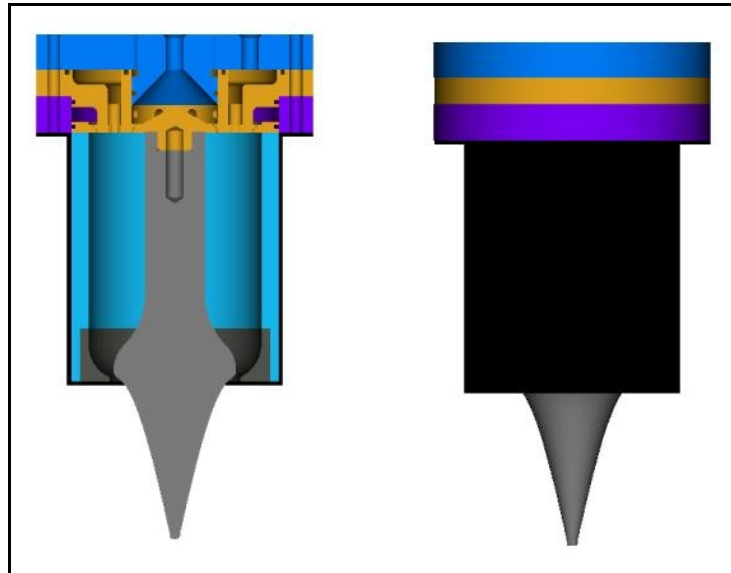


***Figure 4-CAD model of aerospike engine designed, built and tested***

Since erosion rates at the throat of the nozzle would hinder the efficiency of the engine, steps had to be taken to minimize this. Because of its higher melting point, and better tolerance to heat, the spike and the ring creating the throat were made out of graphite. The ability to provide film cooling on both the rod and chamber wall was also important. Therefore, a dual-triplet injector with film cooling was utilized.

### *2.3 Injector Design*

Because of the layout of the spike element being attached to the face of the injector Figure 4, and the high erosion rates of ablative materials, a dual triplet injector with film cooling was most desirable configuration.

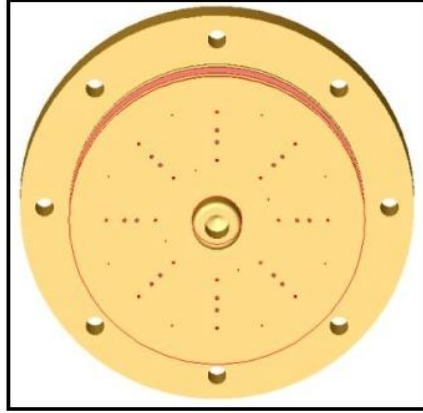


**Figure 5-Dual Triplet Hole Pattern, with Film-Cooling**

Once an injector type is chosen, the sizing of the orifices is achieved with the following procedure. Producing 1,000 lbf of thrust and using a fuel and oxidizer combination of LOX and ethanol are requirements. Given a propellant mixture ratio, reference tables can be consulted to determine the value of the specific impulse. With this data the total weight flow rate can be calculated:

$$\dot{\omega}_{total} = \frac{F}{I_{sp}} \Rightarrow \frac{1000lbf}{240sec} = 4.166667lbf/sec \quad (eq. 2)$$

The oxidizer/fuel (O/F) ratio used is based on equal volume of oxidizer and fuel, which allows the use of identical tanks for the fuel and oxidizer. With equal volumes, the ratio of the density of LOX to the density of ethanol reduces to the mass ratio, which is equal to approximately 1.43. The O/F ratio allows the calculation of the weight flow rate of the oxidizer and fuel:

$$\dot{\omega}_{ox} = \frac{\dot{\omega}_{total} * r}{1 + r} \Rightarrow \frac{4.166667 * 1.43}{2.43} = 2.451989lbf/sec \quad (eq. 3)$$

$$\dot{\omega}_{fuel} = \frac{\dot{\omega}_{total}}{1 + r} \Rightarrow \frac{4.166667}{2.43} = 1.714678lbf/sec \quad (eq. 4)$$

Film cooling flow rates were calculated under the assumption of 30% of the fuel flow allocated to film cooling. A value of 30% was based on past experience using film cooling. 20% of the flow would be concentrated on the outer wall of the combustion chamber, and 10% would be concentrated on the rod, in the center of the combustion chamber. To attain the correct flow rates the injector holes were sized to account for the loss of flow.

$$\dot{w}_{filmcooling} = .30 \times \dot{w}_{fuel} \quad (eq. 5)$$

Orifice areas can then be calculated with the following equation:

$$\dot{\omega} = C_d * A * \sqrt{2 * g * \Delta p * \rho} \Rightarrow A = \frac{\dot{\omega}}{C_d * \sqrt{2 * g * \Delta p * \rho}} \quad (eq. 6)$$

Where  $C_d$  = coefficient of discharge  
 $A$  = Total area of the injector holes  
 $G$  = gravity  
 $\Delta P$  = Change in Pressure  
 $\rho$  = density of fluid  
 $\dot{w}$  = Weight flow rate

#### 2.4 Combustion Chamber

The second major subsystem of a rocket engine is the combustion chamber. The temperature of combustion of the burning propellants is extremely high, approximately 5300 degrees Fahrenheit. This is above the melting temperature of common alloys and therefore thermal insulation must be used to protect any metal surfaces. An ablative lining made from silica cloth and phenolic resin is a cost effective and easy to obtain solution. This lining is a thermal barrier, which absorbs much of the heat by thermally decomposing in an endothermic reaction, and releasing gasses that carry conducted heat away. It also provides oxidation protection by forming a thin layer of molten glass over the surface of the char.

Again, past aerospike engines were designed with several combustion chambers in order to prevent combustion instabilities. However, since this design is at a much smaller scale, a single chamber configuration was chosen and the spike attached to the face of the injector.

The combustion chamber was sized according to three separate requirements flowed-down from the top-level requirements. These included an  $L^*$  of 50 in, where  $L^*$  is a characteristic length and is assumed by previous experience of engine sizing, leading to a chamber volume of 111.48 in<sup>3</sup> using equation 7 from below, and a chamber pressure of 300 psi.

$$V_c = A^* L^* \quad (eq. 7)$$

where  $A^*$  is the throat area and  $L^*$  is the chamber characteristic length. The chamber pressure is based on tank pressure and the  $\Delta P$  across the injector. The propellant tanks were tested at pressures up to 500 psi. This value was one of the major drivers behind the final sizing of the chamber.

Knowing the volume of the chamber allowed for the overall sizing to take place. To find the best sizing for our engine, many factors came into play. The first of these was the diameter of the rod that held the spike in place. This diameter was set at 2 inches for structural reasons. The diameter of the chamber had to take into account enough room for the injector holes (on both sides of the rod), the graphite rod, and the ablative thickness. Allowing at least 1.5 inches on each side of the rod for the injector holes, .5 inches of ablative on each side, and 2 inches for the rod, constrained the diameter to six inches minimum. By varying the chamber length from 6 to 10 inches, and keeping the volume constant, the best-fit diameter was found. This best-fit size, for manufacturing reasons and procurement of the material, was determined to be at 6" inner diameter and 7" length.

#### 2.5 Aerospike Nozzle

The final subsystem of a rocket engine is the nozzle, which is used to transform heat energy into kinetic energy, thus creating a supersonic exhaust velocity. The use of

graphite was employed for the nozzle because of its resistance to extreme temperatures and comparably low erosion rate. Since any significant amount of erosion would change the area of the throat, film cooling was employed as mentioned earlier.

The contour of the nozzle was determined using Ref. 1 (Rao, 1960) for an exit Mach number of 2.71 (Mach number corresponding to an optimum expansion of 12,000 ft for a 300 psi chamber pressure) and an expansion ratio of 5.1. The slope of the throat,  $\theta$ , was based on axisymmetric Prandtl-Meyer expansion.

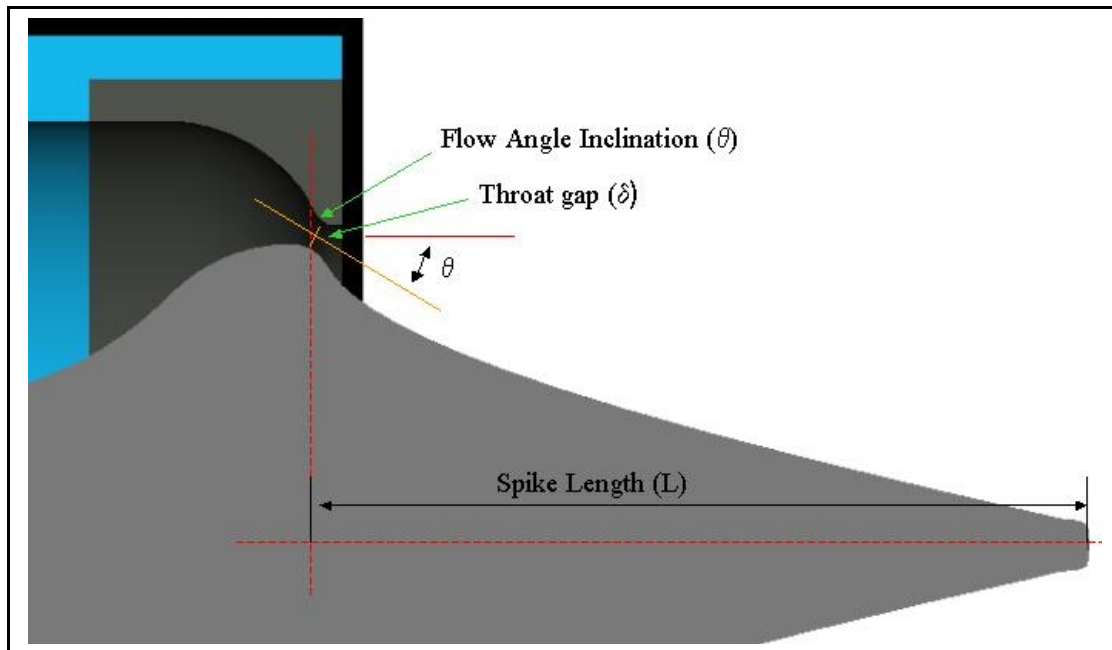


*Figure 6*

### **3.0 Manufacturing**

Since the engine was to be built over a short period of time, planning and scheduling was important in order to meet strict deadlines. Complete parts lists, with the names of vendors and their contact information allowed for smooth procurement of parts.

#### *3.1 Injector*

The most labor intensive phase of manufacturing was machining the injector. One of the most crucial steps was the drilling of small holes, such as the film cooling holes which were .022" diameter, at awkward angles. In order to drill the many small holes that were required (48 overall) a special hand-fed drill chuck was purchased to supplement the mill's capabilities. The complexities of the LOX and fuel manifolds and the connecting passages made the injector a literal maze of canals. Over 100 hours of machining were spent on the injector alone.



***Figure 7-Drilling of injector holes***

### ***3.2 Combustion Chamber***

The combustion chamber housing, consisting of a carbon steel tube and two flanges, was welded together using a MIG welder. Once the housing for the combustion chamber was completed, the ablative liner was made using silica cloth/tape and phenolic resin. Using a mandril, which was machined to the inside dimensions of the ablative liner, the silica tape was doused with phenolic resin and wrapped around the mandril in several layers. Next, the ablative liner was vacuum bagged in order to remove any air bubbles and excess phenolic resin trapped in the silica cloth. After approximately 24 hrs, the liner was removed and the outside diameter was machined to the inside diameter of the chamber. Once machined the steel housing and liner were integrated, which completed the process.



***Figure 8-Machining combustion chamber***

### ***3.3 Aerospike Nozzle and Insert***

Since the contour of the Aerospike nozzle and insert were non-linear, it was machined using a CNC – lathe. A very accurate CAD model of the spike and the

graphite insert were constructed and used to program the cutting commands. A vacuum system was implemented to contain the graphite particles.

## 4.0 Testing

### 4.1 Injector Water Flow Test

The objective of the water flow test was to find the actual pressure drop ( $\Delta P$ ) across the injector. In the design of the engine, the  $\Delta P$  was calculated for both the liquid oxygen injector holes and the fuel injector holes. The  $\Delta P$  values obtained for the liquid oxygen and fuel came out to be 73.1 psi and 90 psi, respectively. The design assumption for the fuel  $\Delta P$  was given at 90 psi and then the LOX  $\Delta P$  was calculated using this value.

The purpose of the water flow test was also to determine if a trim orifice was needed to correct the change in pressure. A trim orifice is a machined ring that is placed inside the Army-Navy (AN) fitting attached to the injector head to widen the outlet in order to allow more flow of propellant. When the flow of propellant is increased the change in pressure across the injector will also increase as shown in the equation below:

$$C_d A = \frac{\dot{W}}{\sqrt{2\rho g \cdot \Delta P}} \quad \Delta P = \left(\frac{\dot{W}}{C_d A}\right)^2 \frac{144}{2\rho g} \quad (eq. 8)$$

*The  $\Delta P$  is calculated by using the fluid properties of water.*

The  $\Delta P$  of the LOX and the fuel will change after the production of the injector due to manufacturing capabilities. In order to obtain the correct  $\Delta P$ , a trim orifice is needed. By using Equation 8, the new diameter of the fitting outlet is determined and can be used to machine the orifice.

The apparatus for the first water flow test included two tanks filled with water. The tanks were then pressurized with helium gas from a separate, third tank. Once the pressure reached the desired amount a valve was released and the water flowed through the injector. A stopwatch recorded the time of the flow and the water was collected in a 5-gallon bucket. Once an arbitrary time was reached, the flow was shut off and the water was weighed on a digital scale. By knowing the time duration of the flow and the weight of the water a weight flow rate could be calculated. Once the data was gathered, the  $C_d$ , or coefficient of discharge, was found using the density of water. Since the  $C_d$  is dimensionless, it could be used again in the calculation of  $\Delta P$  when using the designed flow rate and density of the propellants.

The second water flow test was needed because the first was performed at pressures that created cavitations. For a water flow, the  $\Delta P$  for the pressure entering the injector does not need to be high; therefore a water hose will suffice to provide enough pressure. The second apparatus included a water hose, a pressure gauge, and the injector. When the hose was turned on, the  $\Delta P$  was read off of the pressure gauge and recorded at the desired value. The procedure from this point followed the first flow test by weighing the water and using a stopwatch to record the time. The results from this test are listed below.

---

<sup>1</sup> 144 is used for the conversion factor between psi and ft/s.

**Results:**

<b>Measured Value</b>	<b>Liquid Oxygen Holes</b>
<b>Time</b>	22.31 s
<b><math>\Delta P</math></b>	10 psi
<b>Weight</b>	22.25 lb
<b>Time</b>	19.62 s
<b><math>\Delta P</math></b>	10 psi
<b>Weight</b>	18.31 lb
<b>Time</b>	26.54 s
<b><math>\Delta P</math></b>	10 psi
<b>Weight</b>	26.63 lb

Since the fuel  $\Delta P$  was much higher than the LOX, a trim orifice was used on the LOX side of the injector. An increase of 60 psi was needed on the LOX side to correct the difference between the LOX and the fuel. The Trim was machined out of aluminum alloy and the new  $\Delta P$  for the LOX was calculated at 147.4 psi and 154 psi for the fuel.

The reason for the  $\Delta P$  being off from the calculated values had to do with the manufacturing of the injector. After performing the water test a very large  $\Delta P$  was found, initially. After investigating the problem, it was found that burrs left inside the injector holes retarded the flow, creating a larger  $\Delta P$ . This was repaired by deburring the holes and retesting the injector.

The other main losses came from a combination of the fittings, which connect the propellant lines to the injector, and the dynamic head loss. The dynamic head loss occurred when the flow of propellant entered the injector at 90°, creating a stagnation region and slowing down the flow through the injector.

*4.2 Static Fire Test*

The objective of the static fire test was to validate the design and verify the engine performance. The chamber pressure and the amount of force produced by the engine were recorded and compared to the predicted values.

The static fire test was performed on April 28, 2002 at the Reaction Research Society (RRS) Mojave Test Area (MTA) facility in the Mojave Desert using the static fire test stand provided by Garvey Spacecraft Corporation and funded by The California Launch Vehicle Initiative (CALVEIN). The stand includes a steel structure, two propellant tanks, one for alcohol and one for the LOX, and all the plumbing to supply propellants to the engine. Commands to open and close the propellant valves were sent from a computer that was housed in a near by concrete bunker. This computer also collected data from three 500-lbf load cells, that attached the support stand to the engine to measure the thrust produced, and a pressure transducer on the side of the combustion chamber, which provided chamber pressure (the long ¼ in tube mounted to the side of the combustion chamber can be seen in Figure 10). Figure 9 shows the engine on the test stand ready to be fired.

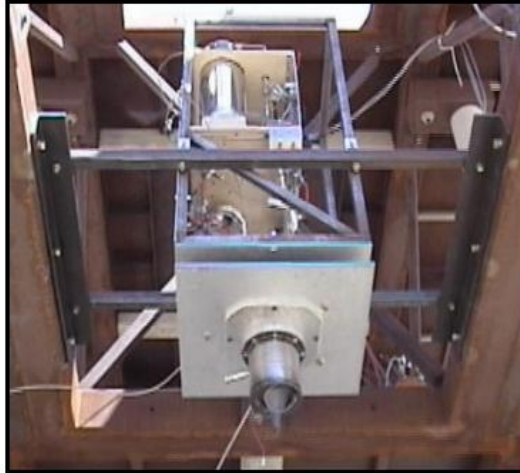


*Figure 9-Aerospike Engine on VTS-2*



*Figure 10*

The engine ignited successfully and began to create the expected flow pattern as is evident in Figure 10 taken 200 ms after ignition. However, right after that, the engine exploded. An investigation of the engine components and slow motion video leads to the belief that the breakage of the spike was the initial point of failure. The pressure acting on the inner surface of the spike forced the spike out of the chamber, which closed off the throat gap. This created a higher pressure in the chamber than in the manifold. The fuel mixture was forced into the injector manifold where it exploded destroying the rest of the engine.



*Figure 11*

The data collected was of limited value for two reasons. First, the sampling rate of the data collection was slow at only 5 samples per second, and second; the engine exploded 200 milliseconds after startup. Due to the low sample rate and the very short burn time little data was actually collected. The data that was obtained is shown in Figure 10.

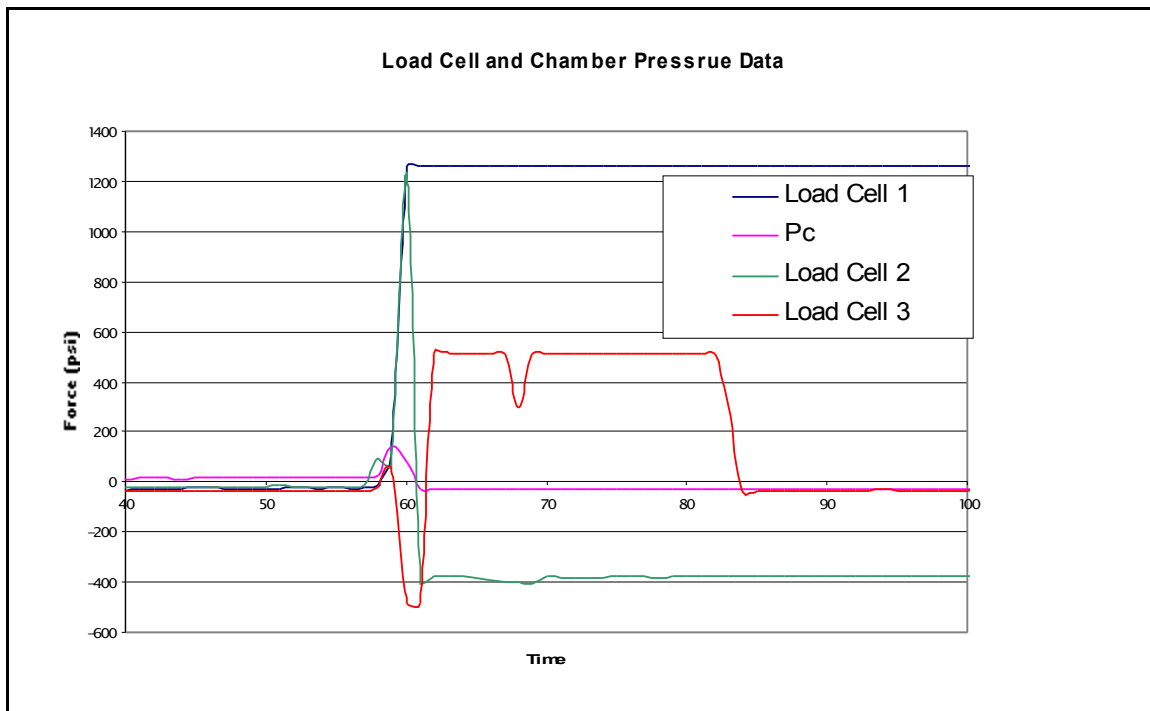


*Figure 12– Load cell data received during static fire*

From Figure 10 it is evident that things did not go as planned. The chamber pressure (Pc) experienced a small rise, about 150 psi, and then fell off. This is probably due to the fact that the chamber had exploded and the pressure transducer was no longer attached nor was it working properly. The first load cell recorded a load of about 1261

lbs at the point of the explosion. Since it was rated to measure 500 lbs, the load cell was probably broken in the explosion and stayed at the point of maximum reading. The load cell was taken apart after the testing and it was found that the strain gauge had actually broken in half. Since the wires were no longer connected, it experienced an infinite load, which kept it at the maximum reading. Load cell 2 experienced the same load at the explosion. However, when this one broke it started to read a negative applied load. This could be due to the fact that when the load cell broke the strain gauge was compressed and read less resistance resulting in the negative reading. The third load cell is interesting because it shows the most activity. It starts off reading the thrust that is initially produced by the engine. It then becomes negative at the explosion. This is probably due to the fact that the explosion created a tension load on this side of the plate resulting in a twisting moment about the center of the plate. After the pieces of the engine fall off of the test stand, the load cell returns to its no load value.

Due to the short burn time and the low data sample rate, the data collected was not very useful. In future tests the data sample rate will be increased with better equipment. This should allow for better data collection.

### **5.0 Conclusion**

The static fire test conducted at the MTA on April 28, 2002 validated most of the design of the aerospike engine. Although the spike nozzle failed structurally, Figure 13 shows that the engine operated successfully, albeit for only 200 ms.



***Figure 13-Left Picture-at  $t=.250$ , Right Picture – at  $t=.500$  (at 30 fps, these are consecutive frames)***

Although the test resulted in the destruction of the hardware and in student disappointment, it also taught students and the rest of the team that the path to success is tortuous and that one should not give up. A test resulting in broken hardware can teach a lot more than paper studies, and emphasizes the balance that needs to be reached between the two.

The team is already working on modifying the plug design and building an improved engine. Static fire test of the modified engine is scheduled to take place at the end of the summer. If the static fire test of the modified engine is successful, the engine will be integrated into the Prospector-2 vehicle (which flew and was recovered back in February) for the first powered flight of an aerospike engine in the history of rocket propulsion development.

### *5.1 The Lessons Learned*

During the water flow testing it became apparent that deburring all of the injector holes greatly decreases the pressure drop across the injector. Therefore, in the future great care will be taken in the deburring of all injector holes in order to achieve the design pressure drop.

It was found that design changes that influence dimensions should be well documented and traced back to all dependants. This should be done to avoid conflicts in part sizes.

It is apparent that more analysis should be done in order to qualify the materials used to manufacture the components. The failure of the graphite spike may have been avoided if more detailed analysis of the forces acting on it and the tensile strength of the material were analyzed.

Looking at the data that was obtained from the static test, it is apparent that a higher sample rate is required in order to achieve more fidelity in the data. This will allow better determination of the failure modes.

### *5.2 Design Changes*

Currently the team is working on design of the second generation aerospike engine taking into consideration the lessons learned from the previous engine. One design consideration would be to incorporate a steel rod through the center of the spike element in order to strengthen it in tension.

Due to the harsh environments of startup, a symmetrical ignition system is in consideration for the next engine. This would help to eliminate some of the unsymmetrical forces that act on the spike during the ignition process.

### References

1. George P. Sutton, Oscar Biblarz Rocket Propulsion Elements, Seventh Edition John Wiley & Sons, Inc, New York, NY. 2001
2. David H. Huang, Dieter K. Huzel (Editor) Modern Engineering for Design of Liquid-Propellant Rocket Engines American Institute of Aeronautics & Astronautics, Reston, VA 1992
3. Giamfranco Angelino Approximate Method for Plug Nozzle Design American Institute of Aeronautics and Astronautics, Reston, VA. 1964.
4. Gabriel D. Roy Advances in Chemical Propulsion: Science to Technology CRC Press, Boca Raton, FL LLC 2001
5. Threshold. Spring 1992. The Boeing Co. 04 November 2001  
<http://www.engineeringatboeing.com/articles/nozzledesign.jsp>
6. G.V.R Rao Spike Nozzle Contour for Optimum Thrust Pergamon Press Inc. New York, NY 1960.

### Acknowledgements

Special thanks to Tom Mueller, Brandy Irish, John Garvey, Eric Besnard, Mike Novratil, Paul Skaar and Mike Fritz